Microstructural analysis and mechanical properties of polycrystalline Ni-rich Ni_3Al alloy prepared by directional solidification

M. Kursa[1]*, J. Malcharcziková[1], J. Pešička[2], V. Vodárek[1], L. Hyspecká[1]

[1] *VŠB-Technical University of Ostrava, Faculty of Metallurgy and Materials Engineering, 17. listopadu 15/2172, CZ-708 33 Ostrava, Czech Republic*
[2] *Charles University, Faculty of Mathematics and Physics, Ke Karlovu 5, CZ-121 16 Prague 2, Czech Republic*

Received 8 August 2008, received in revised form 15 October 2008, accepted 15 October 2008

Abstract

Microstructure and mechanical properties of polycrystalline $Ni_{78}Al_{22}$ alloy prepared by directional solidification (DS) at three growth rates of 18, 60 and 108 mm h^{-1} were studied. After DS the microstructure consisted of coarse columnar $\gamma'(Ni_3Al)$ grains, which solidified directly from the melt, fine γ' grains formed from primary γ-phase (Ni-based solid solution) and γ' nanoparticles formed in the γ channels surrounding fine and coarse γ' grains. Volume fraction of the γ'-phase increased from 70 to 75 vol.% with decreasing growth rate from 108 to 18 mm h^{-1}. The highest room temperature tensile ductility was measured in the specimens with the highest volume fraction of the γ'-phase, which was prepared at the lowest growth rate of 18 mm h^{-1}. After fracture the proportion of the dislocation density in the gauge section to that in the heads was by an order of magnitude higher in the specimens showing the highest ductility than that in the specimens showing the lowest ductility. High values of room temperature ductility result from an intensive multiplication of dislocations during tensile deformation.

K e y w o r d s: nickel aluminides, Ni_3Al, crystal growth, mechanical properties, microstructure

1. Introduction

Polycrystalline near stoichiometric Ni_3Al alloys prepared by melting and casting even from high-purity raw materials are brittle [1, 2]. However, it is possible to achieve good room temperature (RT) ductility by small additions of some elements, such as e.g. boron. On the other hand, Chiba et al. [3] demonstrated that in off-stoichiometric Ni_3Al alloys containing 23 to 26 at.% of Al it was possible to achieve RT ductility without additions of ductilising elements by applying adequate processing techniques consisting of casting, cold-pressing and annealing to obtain a sufficiently ductile re-crystallised polyhedral structure. Another possibility of achieving RT ductility in polycrystalline Ni_3Al alloys is directional solidification (DS) [2, 4–8]. Using combination of both DS and re-crystallisation, it is possible to prepare very thin foils with very good tensile ductility by substantial reduction of thickness up to 95.5 % followed by re-crystallisation [4]. Numerous researchers showed that the grain boundaries and boundary ordering were responsible for different fracture behaviour of Ni_3Al alloys [3, 5, 9]. In polycrystalline near stoichiometric Ni_3Al-alloys prepared by DS, both intragranular and transgranular fracture propagates not only along grain boundaries of $\gamma'(Ni_3Al)$-phase but also along γ'/β(NiAl) or γ'/γ(Ni-based solid solution) interfaces [5, 10]. Analysis of the γ'/γ-phases occurring in various types of Ni-Al based alloys (nickel aluminides and Ni-based superalloys) prepared by DS or by conventional casting was performed by numerous researchers [5, 10–14]. It was shown that intragranular fracture surfaces contained slip traces, while transgranular fracture surfaces contained dimple-like patterns, which is the typical feature of ductile type of fracture [5, 10]. In spite of the fact that positive effect of DS on RT ductility of off-stoichiometric Ni_3Al-based alloys is very well known,

*Corresponding author: tel.: +420 597324501; fax: +420 597321271; e-mail address: kursa.miroslav@vsb.cz

Table 1. Basic data characterising samples of $Ni_{78}Al_{22}$ alloy after directional solidification

R (mm h^{-1})	Grain orientation /deviation/	Ni content (at.%)	Al content (at.%)
108	<221> /5°/	78.7	21.3
60	<311> /8°/	78.3	21.7
18	<111> /4°/	78.3	21.7

more detailed understanding of influence of microstructure on mechanical properties of these alloys is still missing.

The aim of the present work is to study microstructure and mechanical properties of $Ni_{78}Al_{22}$ alloy prepared by DS. Quantitatively determined volume fraction and size of coexisting γ'- and γ-phases and deformation substructures are characterised and related to fracture characteristics.

2. Experimental procedure

Samples of $Ni_{78}Al_{22}$ alloy were prepared by DS at three growth rates R of 18, 60 and 108 mm h^{-1} using Bridgman method under argon atmosphere. Chemical composition of the samples after DS is given in Table 1. Special Al_2O_3 crucibles with apical angle of 60–70°, diameter of 9/11 mm (inner/outer diameter) and length of 120 mm were used for the DS. The sample was placed in a stationary ceramic crucible and after heating to a temperature of 1550 ℃ and dwell of 30 min the heating unit moved along the sample. The temperature gradient in liquid at the solid-liquid interface was measured to vary from 8×10^3 to 10×10^3 K m^{-1}. Crystallographic orientation of columnar grains was measured by Laue X-ray back reflection method on transversal sections to the growth direction. More detailed description of preparation of the samples for Laue X-ray measurements was published recently in the work [6]. As seen in Table 1, the crystallographic orientation of columnar grains is different for individual growth rates.

Tensile specimens with a gauge length of 30 mm and a gauge diameter of 5 mm were prepared by turning and sub-sequential grinding. Tensile tests at room temperature in air were performed at an initial strain rate of 1.15×10^{-4} s^{-1} using a tensile machine INSTRON 5882. Fractographic analysis was performed by scanning electron microscope (SEM) JEOL JSM-6490. Macrostructure and microstructure observations of tensile specimens were performed by optical microscopy [7]. Quantitative image analysis was made on optical microscope OLYMPUS IX 70 equipped with the software "Microimage image Pro 6.2". Volume fractions of coarse (γ'_c) and fine (γ'_f) grains of the γ'-phase were measured on transversal sections oriented perpendicularly to the growth direction. An area of about 2.5 mm^2 was analysed in each sample. Quantitative analysis of fine γ' particles (hereinafter referred as γ'_n nanoparticles), which segregated within the γ channels, was performed on transmission electron microscopy (TEM) micrographs. A lower threshold limit of this analysis was a particle size of about 30 nm. Following relations for distribution functions $f(d)$ and $F(d)$ were used to evaluate mean size of γ'_n particles [15, 16]:

$$f(x) = \frac{1}{\sigma\sqrt{2\pi}} e^{\frac{-(d-\mu)^2}{2\sigma^2}}, \quad (1)$$

$$F(x) = \frac{1}{\sigma\sqrt{2\pi}} \int_{-\infty}^{x} e^{\frac{-(d-\mu)^2}{2\sigma^2}} dx, \quad (2)$$

where d is the diameter of the particle, μ is the mean diameter of particles and σ is standard deviation.

Microanalysis of dual-phase $\gamma + \gamma'$ areas was made by electron microanalyser JCXA-733 equipped with energy dispersive microanalyser EDAX. Substructure of tensile specimens was investigated by TEM using Jeol 2000FX. Foils for TEM observations were prepared from both non-deformed heads and deformed gauge sections of the tensile specimens. Electrolytic thinning of thin foils was realised in an electrolyte composed of 5 % $HClO_4$ and 95 % of CH_3OH at a temperature of −10 ℃ and voltage of 20 V. Dislocation density was evaluated according to relation in the form:

$$\rho = \frac{1}{t}\left\{\frac{\sum n_1}{\sum L_1} + \frac{\sum n_2}{\sum L_2}\right\}, \quad (3)$$

where t is the thickness of thin foil, n_1 is the number of intersections of dislocation lines with lines of regular rectangular mesh for vertical direction, n_2 is the number of intersections of dislocation lines with lines of regular rectangular mesh for horizontal direction, L_1 is the length of mesh lines for vertical direction, L_2 is the length of mesh lines for horizontal direction [17]. The value of t was determined taking into account that majority of dislocation lines lied along ⟨110⟩ crystallographic directions [18]. Foil thickness was calculated on the basis of length of projection of dislocation lines into the plane of the photograph [7].

3. Results

3.1. Microstructure of samples after directional solidification

According to equilibrium binary Ni-Al phase diagram shown in Fig. 1, primary solidification phase in the studied $Ni_{78}Al_{22}$ alloy is the γ-phase. Measured

Table 2. Volume fractions of γ'- and γ-phases V_v in $Ni_{78}Al_{22}$ alloy prepared by DS at various growth rates R

R (mm h^{-1})	Volume fraction V_v (vol.%)				
	Coarse γ'_c grains	Fine γ'_f grains	γ'_n particles	Total of γ'	γ-phase
108	39.9	26.2	4.0	70.1	29.9
60	33.4	34.4	3.0	70.8	29.2
18	46.4	26.4	2.6	75.4	24.6

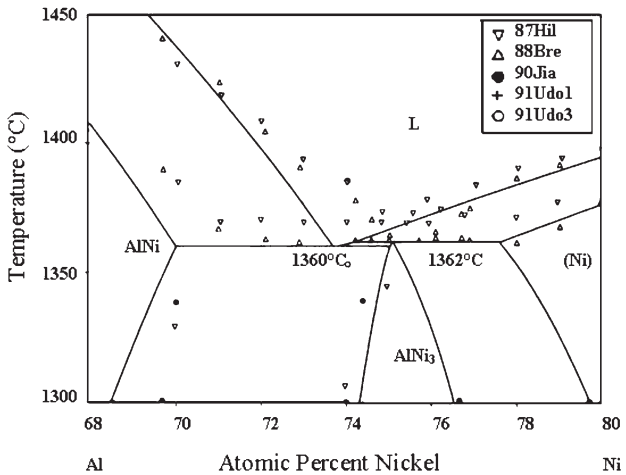

Fig. 1. Binary Ni-Al phase diagram [20].

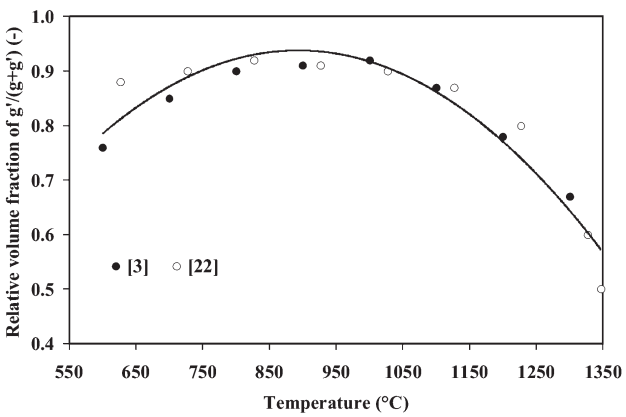

Fig. 2. Equilibrium volume fraction of the γ'-phase as a function of temperature calculated for $Ni_{78}Al_{22}$ alloy from partial equilibrium Ni-Al phase diagrams [3, 21, 22].

chemical compositions of the samples after DS (see Table 1) correspond to a limit content of Al for peritectic reaction at the temperature of 1362 °C [19, 20].

During DS two-phase microstructure consisting of ordered γ'-phase and disordered γ-phase was formed in the samples. Microstructural observations revealed coarse columnar γ'_c grains with a morphology corresponding to solidification from the melt as well as fine γ'_f grains. Volume fractions of γ- and γ'-phases changed during cooling to room temperature, as shown in Table 2. The highest volume fraction of the γ'-phase and the smallest volume fraction of the γ--phase were found in the samples prepared at the slowest growth rate of $R = 18\,\mathrm{mm\,h^{-1}}$. Width of coarse areas of the γ'-phase, i.e. diameter of columnar γ'_c grains, was measured to be about 100 μm and their length of about 1 mm. Figure 2 shows variation of relative volume fraction of the γ'-phase with temperature for the $Ni_{78}Al_{22}$ alloy, which was calculated on the basis of partial binary phase diagrams published elsewhere [3, 21, 22]. As seen in this figure, during cooling the volume fraction of the γ'-phase first increases with decreasing temperature to about 950 °C and then slightly decreases at lower temperature. This phenomenon can be explained by the solubility of Al in the γ-phase. As shown in previous works [21, 22], while solubility of Al in the γ-phase significantly decreases with decreasing temperature, the solubility of Al in the γ'-phase first slightly decreases with decreasing temperature to about of 950 °C and then increases at lower temperatures. Figure 3a shows the typical microstructure of the sample prepared at $R = 18\,\mathrm{mm\,h^{-1}}$. The microstructure consists of a mixture of coarse γ'_c grains and dual phase $\gamma + \gamma'_f$ areas. The dual phase $\gamma + \gamma'_f$ areas were formed from the γ-phase, which solidified directly from the melt. Thickness of the remaining γ channels is about 1 μm. Average size of fine γ'_f grains in dual phase areas was measured to be $8.7 \pm 1.9\,\mu$m. Fine channels of the γ-phase surround γ' grains with the size of $2.3 \pm 0.4\,\mu$m, as seen in Fig. 3b.

Results of EDX microanalysis in selected regions of metallographic transverse sections are given in the Table 3. In all investigated samples, the highest average aluminium content was detected in coarse columnar γ'_c grains and the lowest one was found in the dual phase $\gamma + \gamma'_n$ channels. Aluminium content in the channels is close to the limit of equilibrium solubility of aluminium in this phase. Due to the small thickness of the γ channels that include also γ'_n nanoparticles, measured values for aluminium content are partly affected by a signal from fine γ'_f grains and probably also by the signal from the neighbouring coarse γ'_c grains. Hence, the aluminium content in the γ-phase is probably lower than that shown in Table 3. Figure 4 shows the results of line analysis for Al in dual phase $\gamma + \gamma'_n$

Table 3. Local content of Al in different regions

R (mm h^{-1})	Local content of Al (at.%)		
	Coarse columnar γ'_c grains	Fine γ'_f grains	$\gamma + \gamma'_n$ channels
108	26.6 ± 0.3	24.7 ± 0.3	17.0 ± 0.5
60	25.3 ± 0.2	24.0 ± 0.1	16.6 ± 0.2
18	25.5 ± 0.2	24.0 ± 0.2	16.7 ± 0.2

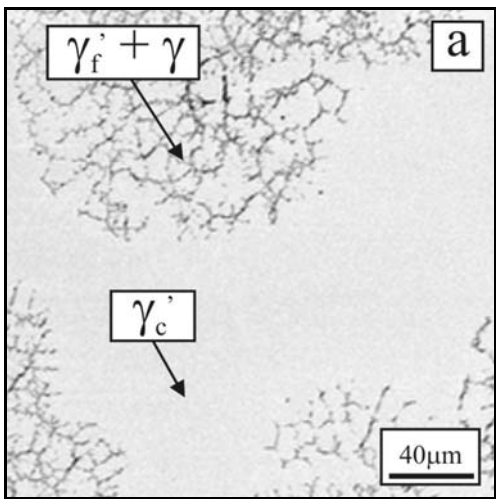

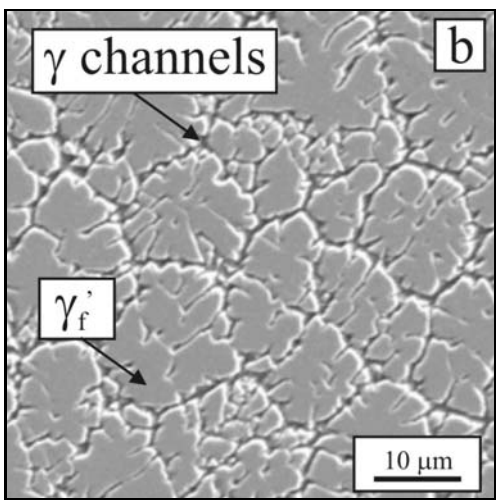

Fig. 3. Microstructure of the sample prepared at $R = 18$ mm h^{-1}, transverse section: (a) coarse γ' grains and related dual phase areas, backscattered SEM, (b) γ channels surrounding fine γ' grains, SEM.

areas. Concentration profile for Al confirms the results shown in Table 3.

3.2. Mechanical properties and deformation microstructures

Figure 5 shows the typical tensile stress-strain curves for three applied growth rates at room temperature. Table 4 summarises 0.2 % offset yield strength (YS), ultimate tensile strength (UTS), plastic elongation to fracture (A) and calculated work hardening exponent n. The lowest values of YS, UTS and A were measured in the tensile specimens prepared at the highest growth rate of $R = 108$ mm h^{-1}. The value of UTS is the highest in the sample prepared at $R = 60$ mm h^{-1}, while ductility is the highest in the sample prepared at the lowest growth rate of $R = 18$ mm h^{-1}. In spite of the fact that the ductility ranging from

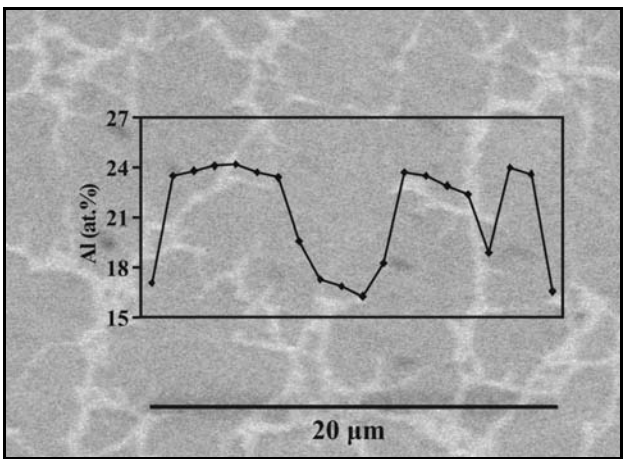

Fig. 4. Concentration profile for aluminium measured along the marked line in dual phase $\gamma + \gamma'_n$ areas, SEM.

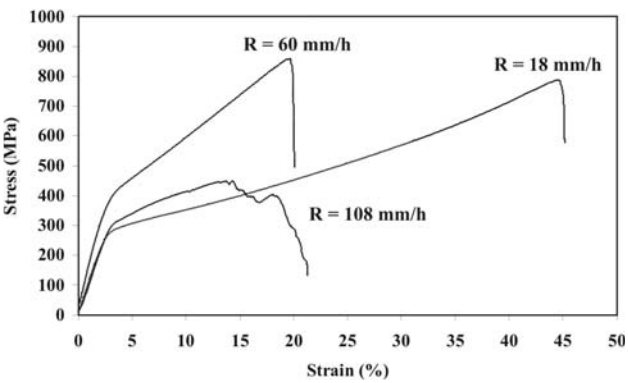

Fig. 5. Tensile stress-strain curves for specimens prepared at $R = 18$ mm h^{-1}, $R = 60$ mm h^{-1} and $R = 108$ mm h^{-1}.

Table 4. Room temperature tensile 0.2 % offset yield strength (YS), ultimate tensile strength (UTS), plastic elongation to fracture (A), work hardening coefficient (n) and Vickers microhardness (HV 0.05) measured at three growth rates

R (mm h^{-1})	YS (MPa)	UTS (MPa)	A (%)	n (–)	HV 0.05
108	267	392	13.9	0.13	268 ± 22
60	343	707	20.5	0.19	269 ± 12
18	245	505	53.4	0.43	262 ± 69

13.9 to 53.4 % is relatively high, even higher values were achieved in a similar polycrystalline alloys by application of DS [4]. The specimen prepared at R = 60 mm h^{-1} was partly fractured in the transition zone between the gauge section and the head, so it cannot be excluded that the fracture initiation was caused by a notch effect, which was formed during machining. Hence, the measured value of plastic deformation to fracture A would be probably higher if the fracture occurred in the gauge section of this specimen. It should be noted that local necking was not observed in the tensile specimens after their fracture. Work hardening coefficient n was determined according to the Hollomon's approximation:

$$\sigma = (k_0 \cdot \varepsilon^n)_{\dot{\varepsilon}=\text{const.}}, \quad (4)$$

where σ is the true stress, k_0 is the material constant, ε is the true strain and $\dot{\varepsilon}$ is the strain rate [23]. The calculated strain hardening coefficients n are summarised in Table 4. The highest value of n was calculated in the specimens prepared at the slowest growth rate of 18 mm h^{-1}.

Table 4 summarises the results of Vickers microhardness measurements (HV 0.05). Disagreement between the evolution of HV 0.05 and evolution of YS, UTS and A with the growth rate is caused by the fact that the tensile properties represent properties of the bulk specimens and the Vickers microhardness characterises properties of very limited micro-volumes. It should be noted that the obtained microhardness values ranging from 262 to 269 are comparable with a value of HV 260 measured in the same alloy prepared by DS [5].

Figure 6 shows the typical fracture features of the tensile specimens. The fracture crack propagated intragranularly as well as transgranularly showing slip traces at the fracture surfaces (Fig. 6a). Figure 6b clearly shows dimples on the fracture surface, which is the typical fracture feature of a ductile type of fracture. Morphology of the dimples with an average size of 2.3 ± 0.3 μm was sometimes cubic indicating cuboidal morphology of γ' particles.

Figure 7 shows the typical examples of dislocation sub-structure within the γ'_c grains in the head and gauge section of a tensile specimen prepared at R = 18 mm h^{-1}. Pairs of dislocations (super-dislocations)

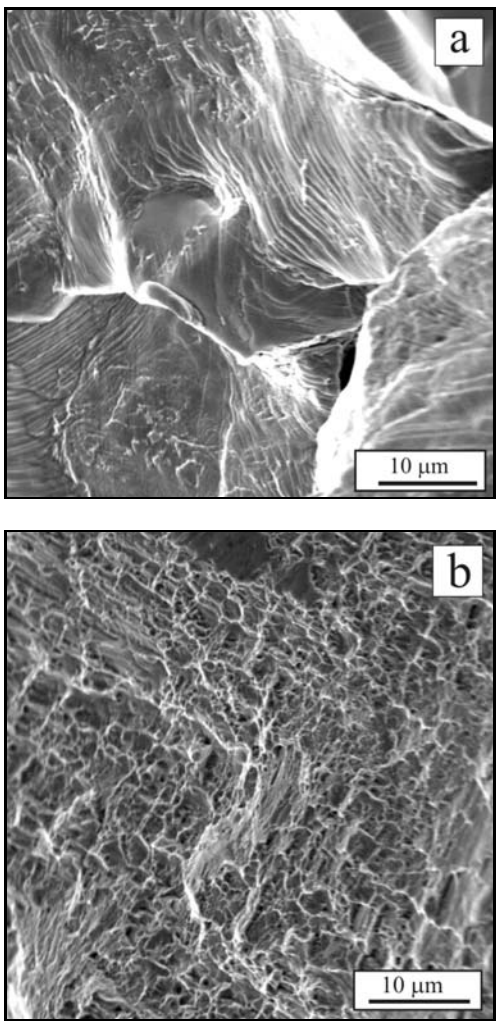

Fig. 6. SEM micrographs showing fracture surface of tensile specimen prepared at R = 18 mm h^{-1}: (a) intragranular fracture with traces of slip bands, (b) transgranular ductile fracture mode with dimples.

are locally observed in the ordered γ'-phase, as seen in Fig. 7a. In the gauge section of the specimen, the dislocation density was higher by one order of magnitude, as shown in Fig. 7b. The following trends can be derived from the TEM observations:

a) dislocation density in coarse γ'_c grains decreases with decreasing growth rate,

b) dislocation density in the gauge section of in-

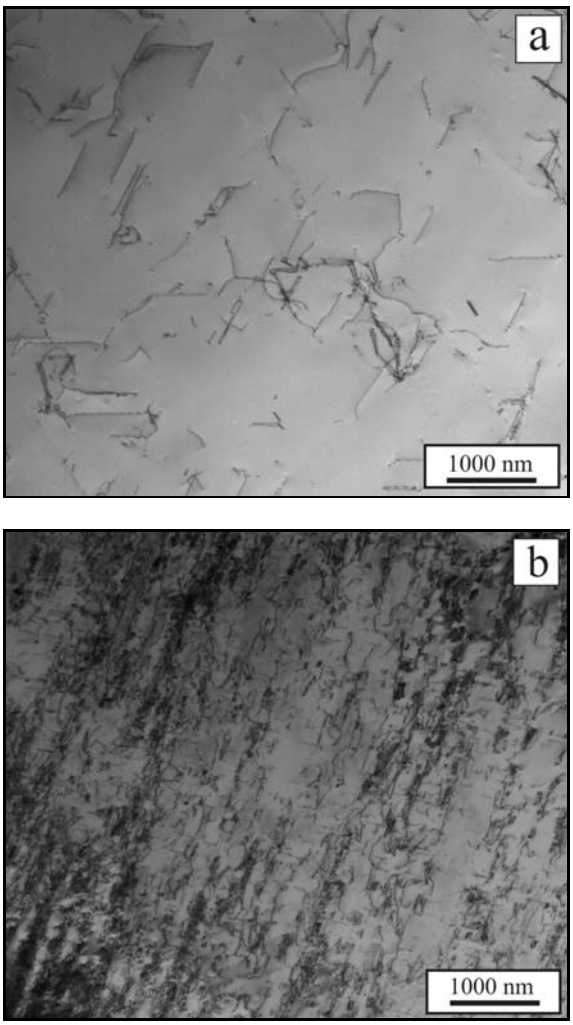

Fig. 7. TEM micrographs showing dislocation substructure within the γ_c' grains in tensile specimen prepared at $R = 18\,\mathrm{mm\,h^{-1}}$ after fracture: (a) head of the specimen, (b) gauge section of the specimen.

dividual testing specimens is approximately by one order of magnitude higher than that in the heads of specimens.

The results of evaluation of dislocation density in the coarse γ_c' grains in both the heads and gauge sections of tensile specimens are summarised in Table 5. The proportion ρ_p/ρ_0 of dislocation density in the gauge section ρ_p to that in the head ρ_0 was the highest one in the specimens exhibiting the highest ductility values ($R = 108\,\mathrm{mm\,h^{-1}}$). The measured values of dislocation density correspond approximately to those obtained for $Ni_{75}Al_{22}Hf$ alloy after plastic deformation at a temperature of 84 ℃ [24]. The dislocation density in the area of fine γ_f' grains and in the $\gamma + \gamma_n'$ channels was lower than that in the areas with columnar γ_c' grains.

Figure 8 shows TEM substructure formed in dual phase $\gamma + \gamma_n'$ channels of the specimen prepared at R

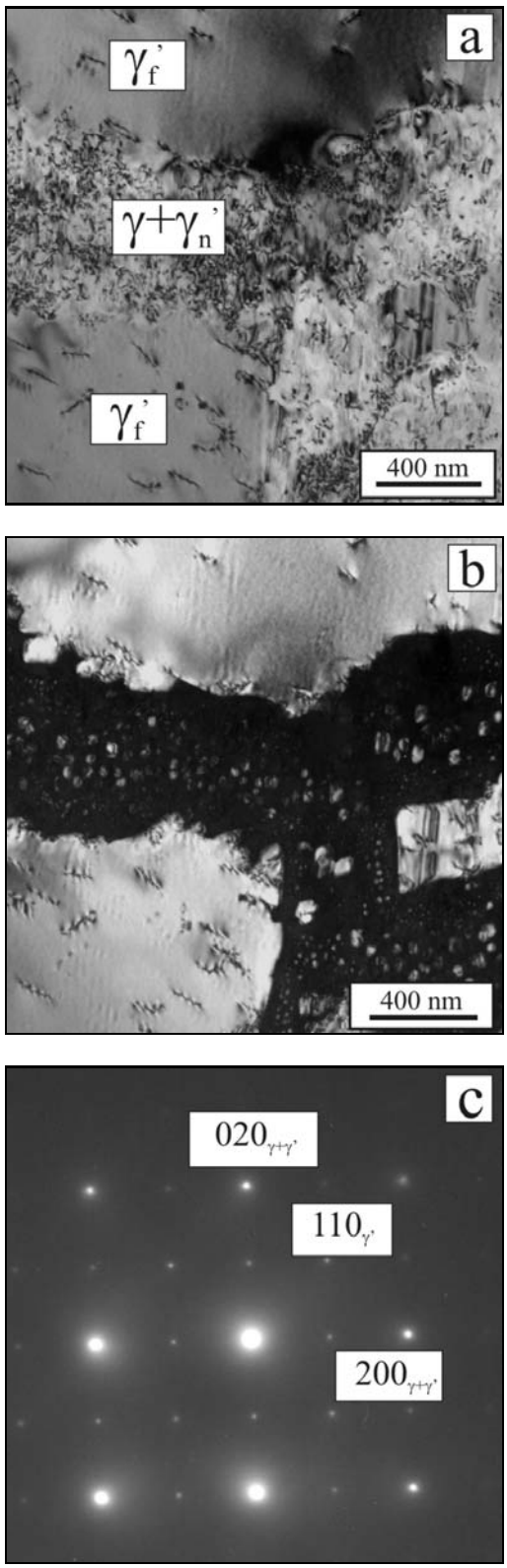

Fig. 8. TEM micrograph showing substructure in dual phase $\gamma + \gamma_n'$ area of tensile specimen prepared at $R = 108\,\mathrm{mm\,h^{-1}}$: (a) projection in bright field, (b) projection in dark field in supra-structural reflexion $110_{\gamma'}$, (c) selected area diffraction (SAD) pattern from $[001]_{\gamma+\gamma'}$.

Table 5. Dislocation density in the heads (ρ_0), gauge sections (ρ_P) and proportion ρ_P/ρ_0 in fractured tensile specimens prepared at three growth rates R

R (mm h^{-1})	ρ_0 (10^{13} m^{-2})	ρ_P (10^{13} m^{-2})	(ρ_P/ρ_0)
108	1.2	6.1	5.1
60	0.8	13.7	17.1
18	0.3	10.8	36.0

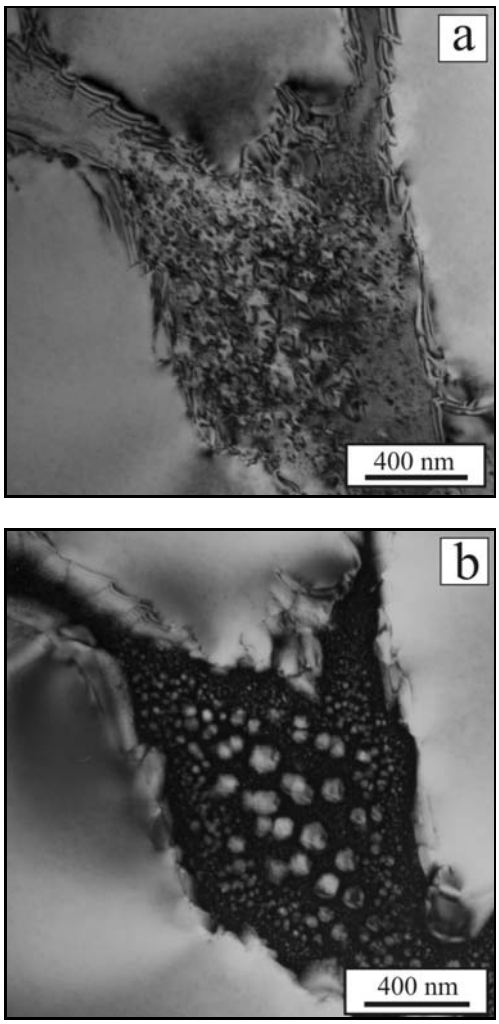

Fig. 9. TEM micrograph showing substructure in dual phase $\gamma + \gamma'_n$ area of tensile specimen prepared at R = 18 mm h^{-1}: (a) projection in bright field, (b) projection in dark field in supra-structural reflexion $100_{\gamma'}$.

= 108 mm h^{-1}. Formation of the γ' particles within the γ channels is not clearly visible using bright field contrast, as seen in Fig. 8a. On the other hand, projection in dark field, which was made in supra-structural reflexion $110_{\gamma'}$, shows clearly γ'_n nanoparticles distributed within the γ channels, as seen in Fig. 8b. Square morphology of γ' particles often with rounded corners

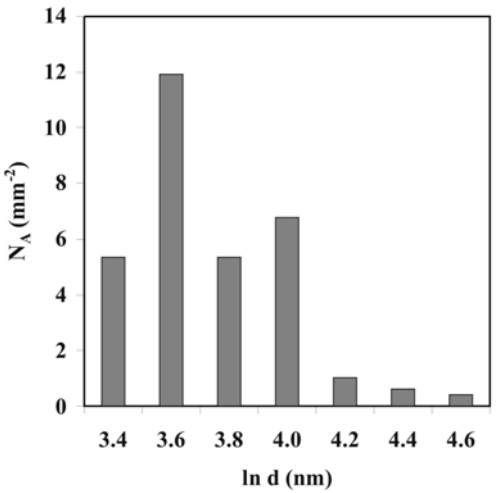

Fig. 10. Dependence of number of γ' particles per surface unit of the γ-phase N_A on edge length of the γ' particles d in tensile specimen prepared at R = 18 mm h^{-1}.

and protuberant edges indicate that these particles are cubes. Onaka et al. [25] made a simplified energy analysis and proved that such morphological features were typical for coherent γ' particles in the γ-phase. Figure 8c shows selected area diffraction (SAD) pattern with only basic and super-structure reflexions of the γ'-phase in dual phase $\gamma + \gamma'_n$ areas. The absence of "extra" reflexions of the γ-phase in the diffraction $\gamma + \gamma'$ patterns is related to the following phenomena:

a) $\gamma'(Ni_3Al)$-phase has a structure of the $L1_2$ (Pm3m) type with lattice parameter of a = 0.356 nm and γ-phase has a structure of A1 (Fm3m) type with lattice parameter a = 0.352 nm.

b) Between both phases there exists crystallographic orientation relation "cube to cube".

These facts result in mutual overlap of hkl* reflexions of both phases in diffraction patterns. The size of the γ' particles was larger (about 150 nm) in the middle of the γ channels and decreased toward the γ/γ'_f boundaries, as seen on Fig. 9. Volume fraction of γ'_n particles in the γ channels decreased with decreasing growth rate. Precipitation of the γ'_n particles in the γ-phase results from a change of aluminium solubility in the γ-phase with decreasing temperature. Change of the size of the γ'_n particles within the thickness of γ channels is caused probably by the concentration gradient of aluminium in these regions.

Figure 10 shows dependence of number of γ' particles per surface unit of the γ-phase N_A on edge length of the γ' particles d for the specimen prepared at R = 18 mm h^{-1}. This figure indicates the possibility of bi-modal size distribution of the γ'_n particles located in the γ channels similar to that reported by Hakl et al. [14] in nickel-based superalloy IN 792 5A.

4. Discussion

Directional solidification can be successfully used for production of Ni-rich Ni_3Al-based alloys with columnar grain structure and good RT ductility. Slip traces on intragranular and transgranular dimple-like ductile fracture surfaces support high obtained values of ductility of the studied alloy. Nevertheless, improved RT ductility can be achieved in inherently brittle Al-rich Ni_3Al-based alloys with dual phase γ'/β(NiAl) structure prepared also by directional solidification [5, 10, 26, 27]. In these alloys, fracture crack propagates in intragranular and transgranular manner, more frequently along the γ'/β than γ'/γ' boundaries. Surprisingly, even the presence of sulphur at the grain boundaries does not cause brittle fracture, when such alloys are prepared by DS [28]. Hence, there is a similarity between fracture behaviour and ductility of polyhedral Ni_3Al-based alloys prepared by directional solidification with chemical composition close to either hypo- or hyper-stoichiometric composition.

In the case of the studied $Ni_{78}Al_{22}$ alloy, coarse γ' grains were formed from the melt by a peritectic reaction and they filled the space between already solidified crystals of the γ-phase. This is supported by the fact that aluminium content in the coarse γ' grains is higher than that in fine γ' grains (see Table 3). This can be explained by the binary phase diagram showing that the γ'-phase formed from the melt can contain up to 26 at.% of Al at the peritectic temperature, while during precipitation from the γ-phase it can contain maximum 25 at.% of Al [19, 20]. The volume fraction of the γ'-phase gradually increases during cooling to a temperature of about 950 ℃ (Fig. 3) due to formation of fine γ'_f grains from the disordered γ-phase. Average aluminium content is lower in fine grains (24.0 at.%), since aluminium content in the γ'-phase slightly decreases to about 22.4 at.% of Al at 950 ℃. At temperatures below 950 ℃, the aluminium content in the γ'-phase again slightly increases, as it follows from the part of the binary phase diagram [3, 21, 22].

Cooling rates influence the microstructure significantly, particularly volume fractions, size, degree of ordering and local chemical composition of the γ'- and γ-phases in Ni_3Al-based alloys [9]. The studied $Ni_{78}Al_{22}$ alloy shows similar behaviour, e.g. volume fraction of coarse columnar γ'_c grains is the highest one and fraction of the γ'_n nanoparticles in the γ-phase is the smallest one for the slowest growth rate. The fact that the largest size of the γ'_n nanoparticles is observed in the central parts of the γ channels (see Fig. 8) can be explained by their dissolution and consequently by re-distribution of Al during cooling in the temperature interval, where the volume fraction of γ'-phase again decreases (see Fig. 2). Dual phase $\gamma + \gamma'_n$ channels are comparatively narrow (about 1 μm), which allows dissolution of small γ'_n nanoparticles and diffusion of Al to larger ones. Previously published results on concentration profiles for Al along Ni/Ni_3Al interfaces support this statement [22, 29]. Volume fraction of γ'_n nanoparticles in the γ-phase is very small in comparison with fine and coarse columnar γ' grains and it decreases with decreasing growth rate (see Table 2). This means that these particles do not have decisive influence on the fracture behaviour of the $Ni_{78}Al_{22}$ alloy. Figure 3b shows dual phase channels penetrating into fine γ'_f grains, which disintegrate them to smaller γ' particles with a size of $d = 2.3 \pm 0.4\,\mu$m. The shape and size of such γ' particles is similar to quadratic-like dimples observed on fracture surfaces (Fig. 6). Facets drawn above the dimples are therefore probably dual phase $(\gamma + \gamma'_n)$ channels. However, the portion of such dimple-like fracture surface was not evaluated quantitatively and it was not compared with the volume fraction of dual phase areas and fine γ'_f grains.

Volume fraction of the γ'-phase is close to an optimal value ranging from 60 to 70 vol.%, stated for obtaining high creep resistance at high temperatures in Ni-based superalloys [4, 14, 30, 31]. Volume fraction of coarse columnar grains was the highest in the specimen prepared at $R = 18\,\mathrm{mm\,h^{-1}}$, which showed the highest ductility. Work hardening coefficient n increases with decreasing growth rate (see Table 4). It is known that the work hardening coefficient is high in Ni_3Al single crystals as well as in some Ni_3Al-based alloys and approaching a value of $n = 0.5$ [32]. Therefore, high value of the work hardening coefficient of 0.43 measured for the studied alloy can be connected with high volume fraction of coarse γ'_c grains, which control the plastic deformation of the specimens prepared at $R = 18\,\mathrm{mm\,h^{-1}}$ [5, 32]. Assuming measured dislocation densities in the investigated tensile specimens prepared at $R = 18\,\mathrm{mm\,h^{-1}}$ leads to a conclusion, that multiplication of dislocations, mobility of dislocations and overcoming the barriers such as grain boundaries by dislocations contributed to high RT ductility. Multiplication of dislocations was also recently determined as the main factor responsible for anomalous increase of the yield strength with increasing temperature [25].

5. Conclusions

The investigation of the microstructure and mechanical properties of $Ni_{78}Al_{22}$ alloy prepared by DS suggests the following conclusions:

1. After DS the microstructure of the studied alloy consists of coarse γ'_c grains, fine γ'_f grains and channels of γ-phase. In the γ channels, formation of γ'_n nanoparticles was observed. The size of γ'_n nanoparticles decreases from the middle regions of the γ channels towards γ/γ'_f boundaries.

2. Total volume fraction of the γ'-phase varied between 70 to 75 vol.%. The highest volume fraction

of the γ'-phase was measured in the samples prepared at the slowest growth rate. Volume fractions of coarse γ'_c grains and γ'_n nanoparticles grains represent the largest and the lowest proportion of the measured total volume fraction of the γ'-phase in the studied alloy, respectively.

3. The proportion of dislocation density in the gauge section to that in the head was the highest one in the tensile specimens prepared at the slowest growth rate, in which the ductility achieved the highest value. The main factor responsible for high RT ductility is multiplication of dislocations during tensile deformation.

Acknowledgements

The presented results were obtained within the frame of the research project MSM 6198910013 "Processes of preparation and properties of high-purity and structurally defined special materials".

References

[1] SAUTHOFF, G.: Intermetallics. Weinheim, Germany, VCH Verlagsgesellschaft 1995.
[2] KURSA, M.: Transactions of the VŠB-Technical University of Ostrava, Metallurgical Series, *46*, 2000, p. 144.
[3] CHIBA, A.—HANADA, S.—WATANABE, S.—OBANA, T.—TANOSAKI, K.—FUJITA, M.: Mater. Trans. JIM, *33*, 1992, p. 503.
[4] DEMURA, M.—SUGA, Y.—UMEZAWA, O.—KISHIDA, K.—GEORGE E. P.—HIRANO, T.: Intermetallics, *9*, 2001, p. 157.
[5] BORODIANSKA, H.—DEMURA, M.—KISHIDA, K.—HIRANO, T.: Intermetallics, *10*, 2002, p. 255.
[6] MALCHARCZIKOVÁ, J.—KURSA, M.—BELJAJEV, I. V.: Acta Metall. Slov., *12*, 2006, p. 427.
[7] MALCHARCZIKOVÁ, J.—KURSA, M.—BELJAJEV, I.V.: Acta Metall. Slov., *13*, 2007, p. 658.
[8] LAPIN, J.—BAJANA, O.: Kovove Mater., *43*, 2005, p. 169.
[9] BARROS, A. M.—TENÓRIO, J. A. S.: Intermetallics, *13,* 2005, p. 137.
[10] GEORGE, E. P.—IMAI, M.—HIRANO, T.: Intermetallics, *5*, 1997, p. 425.
[11] LAPIN, J.—MAREČEK, J.—KURSA, M. : Kovove Mater., *44*, 2006, p. 1.
[12] FLORIAN, M.: Kovove Mater., *41*, 2003, p. 73.
[13] FLORIAN, M.: Kovove Mater., *38*, 2000, p. 305.
[14] HAKL, J.—VLASÁK, T.—LAPIN, J.: Kovove Mater., *45*, 2007, p. 177.
[15] BAILLARGEON, G.: Methodes statistiques de l'ingénieur. Vol. 1. Paris, SMG 1990.
[16] UNDERWOOD, E. E.: Quantitative Stereology. Menlo Park California, USA, Addison-Wesley Publ. Corp 1970.
[17] WILLIAMS, D. B.—CARTER, C. B.: Transmission Electron Microscopy. NY, Plenum Press 1996.
[18] KRUML, T.—VIGUIER, B.—BONNEVILLE, J.—MARTIN, J. L.: Mat. Sci. Eng. A, *234–236*, 1997, p. 755.
[19] MASSALSKI, T. B.: Binary Alloys Phase Diagrams. Ohio, ASM International 1986 and CD ROM, version 1.0, 1996.
[20] MICHNA, Š. et al.: Encyclopaedia of Aluminium. Prešov, Adin 2005 (in Slovak).
[21] WATANABE, M. et al.: Acta Metall. Mater., *42*, 1994, p. 3381.
[22] DRÁPALA, J.—TRUNČÍK, M.—KURSA, M.—DAGBERT, C.—HYSPECKÁ, L.: Jnl. Electrical Engineering, *48*, 1997, p. 81.
[23] POKLUDA, J.—KROUPA, F.—OBDRŽÁLEK, L.: Mechanical properties and structure of solid substances. Technical University in Brno, PC-DIR, spol. s r.o. 1994, p. 383 (in Czech).
[24] KRUML, T.—PAIDAR, V.—MARTIN, J. L.: Intermetallics, *8*, 2000, p. 729.
[25] ONAKA, S.—KOBAYASHI, N.—FUJII, T.—KATO, M.: Intermetallics, *10*, 2002, p. 343.
[26] LAPIN, J.: Intermetallics, *14*, 2006, p. 1417.
[27] LAPIN, J.—PELACHOVÁ, T.—BAJANA, O.: Intermetallics, *8*, 2000, p. 1417.
[28] GEORGE, E. P.—IMAI, M.—HIRANO, T.: Intermetallics, *5*, 1997, p. 425.
[29] LOSERTOVÁ, M.—HYSPECKÁ, L.—SOZAŃSKA, M.—ADAMIEC, J.: Degradacja połączenia Ni_3Al-Ni pod wpływem dyfuzji aluminium. No. 1, Sigma 2005 (in Polish).
[30] CORMIER, J.—MILHET, X.—CHAMPION, J. L.—MENDEZ, J.: Adv. Eng. Mat., *10*, 2008, p. 56.
[31] KUNZ, L.—LUKÁŠ, P.—MINTÁCH, P.—HRBÁČEK, K.: Kovove Mater., *44*, 2006, p. 275.
[32] LAPIN, J.: Intermetallics, *5*, 1997, p. 615.